frontiers | Frontiers in Energy Research

TYPE Original Research
PUBLISHED 21 November 2024
DOI 10.3389/fenrg.2024.1485241

OPEN ACCESS

EDITED BY
Zequn Yang,
Central South University, China

REVIEWED BY
Ying Teng,
Shenzhen University, China
Jiajun He,
University of Illinois at Urbana-Champaign, United States

*CORRESPONDENCE
Jishi Geng,
gengjishi@cumt.edu.cn

RECEIVED 23 August 2024
ACCEPTED 11 November 2024
PUBLISHED 21 November 2024

CITATION
Huang H, Sun Q, Yang D, Geng J, Zhang L and Pan Y (2024) Effects of CO_2–water–rock cycling cycles on sandstone pore structure. *Front. Energy Res.* 12:1485241. doi: 10.3389/fenrg.2024.1485241

Effects of CO_2–water–rock cycling cycles on sandstone pore structure

Hao Huang[1], Qiang Sun[1,2,3], Duoxing Yang[4], Jishi Geng[1]*, Liwei Zhang[5,6] and Yanning Pan[1,7]

[1]College of Geology and Environment, Xi'an University of Science and Technology, Xi'an, Shaanxi, China, [2]Shaanxi Provincial Key Laboratory of Geological Support for Coal Green Exploitation, Xi'an, China, [3]Key Laboratory of Coal Resources Exploration and Comprehensive Utilization, Ministry of Land and Resources, Xi'an, China, [4]National Institute of Natural Hazards, Ministry of Emergency Management of China, Beijing, China, [5]State Key Laboratory of Geomechanics and Geotechnical Engineering, Institute of Rock and Soil Mechanics, Chinese Academy of Sciences, Wuhan, China, [6]University of Chinese Academy of Sciences, Beijing, China, [7]China School of Earth Science and Resources, Chang'an University, Xi'an, China

As global CO_2 levels increase, the storage of CO_2 in saline aquifers is considered a large-scale and cost-effective method for mitigating CO_2 emissions. To examine the impact of cyclic CO_2 injection on sandstone formations within various saline aquifers, five cyclic injections of differing durations were performed, and the effects of the frequency and duration of CO_2 injection cycles on sandstone pore structure were monitored using nuclear magnetic resonance. Additionally, ICP-OES was employed to assess changes in the total dissolved solids and metal ion concentrations in the saline water layer post-injection. The findings reveal that sandstone samples experience structural degradation as a result of cyclic injection. Initially, the proportion of macropores in sandstone samples increases with the number of injections but subsequently decreases. SO_4^{2-} ions exert a more significant influence on the sandstone pore structure compared to Cl^-ions. The concentrations of Ca^{2+} and Mg^{2+} ions in the solution initially rise, followed by a subsequent decline. By integrating the principles of pore structure and considering the formation of crystals through the combination of metal cations and anions, the mechanism underlying the changes in sandstone pore structure due to cyclic injection is elucidated. This study explores the effects of CO_2 cyclic injection on reservoir sandstone and evaluates how different saline aquifer types affect pore structure deterioration. The research offers valuable reference points and a foundation for laboratory investigations of underground CO_2 storage in saline aquifers.

KEYWORDS

CO2-water-rock, sandstone, pore structure, ic-oes, NMR

1 Introduction

With the progression of industrialization, greenhouse gas emissions have risen significantly, with carbon dioxide (CO_2) emerging as the most critical greenhouse gas (GHG) due to its sharply increasing atmospheric concentration (McGlade and Ekins, 2015; Ou et al., 2021). The rise in GHG levels has contributed to global warming, resulting in a range of environmental and ecological issues such as

polar glacier melting, increased frequency of extreme weather events, and seawater acidification, all of which present substantial risks to human survival and safety (Seneviratne et al., 2016; Baker et al., 2018). In response to these climate change challenges, there has been a global effort to explore and adopt advanced technologies for greenhouse gas reduction, among which CCUS technology, particularly the underground saline aquifer storage method, has gained considerable attention (Aminu et al., 2017; Dou et al., 2023).

Carbon capture, utilization, and storage (CCUS) technology is regarded as a crucial solution for mitigating global warming, with underground saline aquifer storage receiving notable attention due to its high storage capacity, minimal environmental impact, and advanced technological development (Zhang et al., 2016). Numerous pilot projects have been conducted to explore this method. Research into CO_2 storage in brackish aquifers indicates that key parameters affecting CO_2 storage include porosity, permeability, temperature, injection pressure, injection rate, type of brackish aquifer, mineralization, and so on (Bachu and Bennion, 2008; Lv et al., 2017; Kumar et al., 2020; Tawiah et al., 2021; Tang et al., 2023). Basalt permeability varies significantly with CO_2 fluid injection rates, exhibiting a slight decrease at low flow rates and an increase at high flow rates (Luhmann et al., 2017). In siltstone samples saturated with CO_2 and high saltwater concentrations, salt precipitation in rock pores notably reduced siltstone permeability (Jayasekara et al., 2020). CO_2-brine interactions in carbonate rocks increase grain roughness, create more micro- and macropores, and decrease the volume of intermediate pores (Thaysen et al., 2017; Seyyedi et al., 2020). Supercritical CO_2 reacts with brine to form carbonic acid, which interacts with calcite, leading to increased porosity and permeability in chert. However, the continuous deposition of Ca^{2+} and Mg^{2+} in brine decreases limestone porosity and permeability (Yang et al., 2020; Xu et al., 2022). Regardless of the initial geochemical equilibrium of the underground saline aquifer prior to CO_2 injection, carbon sequestration operations disrupt the original equilibrium, initiating a series of mineral dissolution and regeneration reactions. The complexity of CO_2 injection processes is amplified by high-pressure and high-temperature conditions in deep saline aquifers (Kim and Santamarina, 2014; Venkatraman et al., 2017). Previous studies conducted substantial studies on the storage of CO_2 in saline formations, focusing on various types of core samples, which provided valuable theoretical guidance for carbon sequestration experiments. However, the rapid dissolution of CO_2 into formation brine and the poor flow characteristics of nearly saturated CO_2 solutions indicate that repeated injection is a viable strategy. Furthermore, the CO_2 sequestration capacity is significantly influenced by the injection scheme, with alternating injection greatly enhancing the brine's capacity to capture CO_2 (Al-Khdheeawi et al., 2019; Wang et al., 2020). This study offers supplementary research in this area.

To investigate the evolution of sandstone reservoir pore structure during the injection cycle, Na_2SO_4-type and NaCl-type brines are used to simulate representative subsurface brine environments, with a deionized water group established as a control. This setup allows for a comprehensive assessment of the effects of different brine types on sandstone pore structure. By systematically analyzing the pore change mechanism during the cyclic injection process, the study reveals the micro-adjustments in pore structure resulting from the interaction between carbon dioxide and saltwater. The findings provide valuable laboratory data and theoretical insights for optimizing injection strategies, enhancing sequestration efficiency, and guiding practical applications of carbon sequestration projects in underground saline aquifers. This research is crucial for advancing carbon sequestration technology and achieving global carbon emission reduction goals.

2 Methods and materials

2.1 Materials

The sandstone samples for this study were sourced from Erdos City, Inner Mongolia Province, China, as illustrated in Figure 1. To determine the precise composition and microstructural features of the samples, X-ray diffraction (XRD) and petrographic thin section analyses were performed, as shown in Figure 2. Petrographic thin-section observations indicated that the sandstone primarily consists of quartz, feldspar, calcite, and rock fragments (Table 1). Quartz shows no secondary enlargement, and the grains exhibit clear contacts with good sorting. The rock samples, cut from drill cores at the same depth, were prepared into cylindrical samples with dimensions of $\Phi 25 \times 50$ mm. These samples were placed in a drying oven for 24 h prior to measuring their density and porosity. Samples with similar densities and porosities were selected for the cyclic tests, and their densities and porosities are detailed in Table 2.

2.2 CO_2-water-rock cycle test procedure

To investigate the effects of water evaporation and salt precipitation on reservoir rocks during intermittent CO_2 injection and sequestration in underground saline aquifers, a laboratory simulation experiment was designed to study the changes in pore structure of reservoir rocks after intermittent CO_2 injection. This study aims to evaluate the long-term safety and effectiveness of sequestration technologies. A reaction setup was constructed (see Figure 3) to simulate geothermal conditions and the characteristics of underground saline aquifers. The samples were categorized into three groups based on saline water type: Na_2SO_4, NaCl, and a control group with deionized water. The saline solutions were prepared using deionized water at a concentration of 30 g/L (30,000 ppm), with specific parameters detailed in Table 3. Research indicates that deep saline aquifers at depths of 800–2,000 m with salinity levels of 20,000–250,000 ppm are optimal for CO_2 geological sequestration (Fang et al., 2016; Boampong et al., 2023). The experimental procedure is outlined in Figure 4. Initially, the solutions and dried rock samples underwent oversaturation treatment (vacuum pressure saturation) to simulate real formation conditions. The saturated samples were then placed in the reaction setup at 40 °C and 5 MPa. After the designated reaction times, the samples were retrieved for nuclear magnetic resonance (NMR) scanning, and the solution was analyzed using inductively coupled plasma-optical emission spectrometry (ICP-OES) to measure changes in pore space and ion concentration in the reacted rock samples. Finally, wave velocity, dry mass, metal ion concentration in the solution, and total dissolved solids (TDS) of the samples were recorded. This process constituted

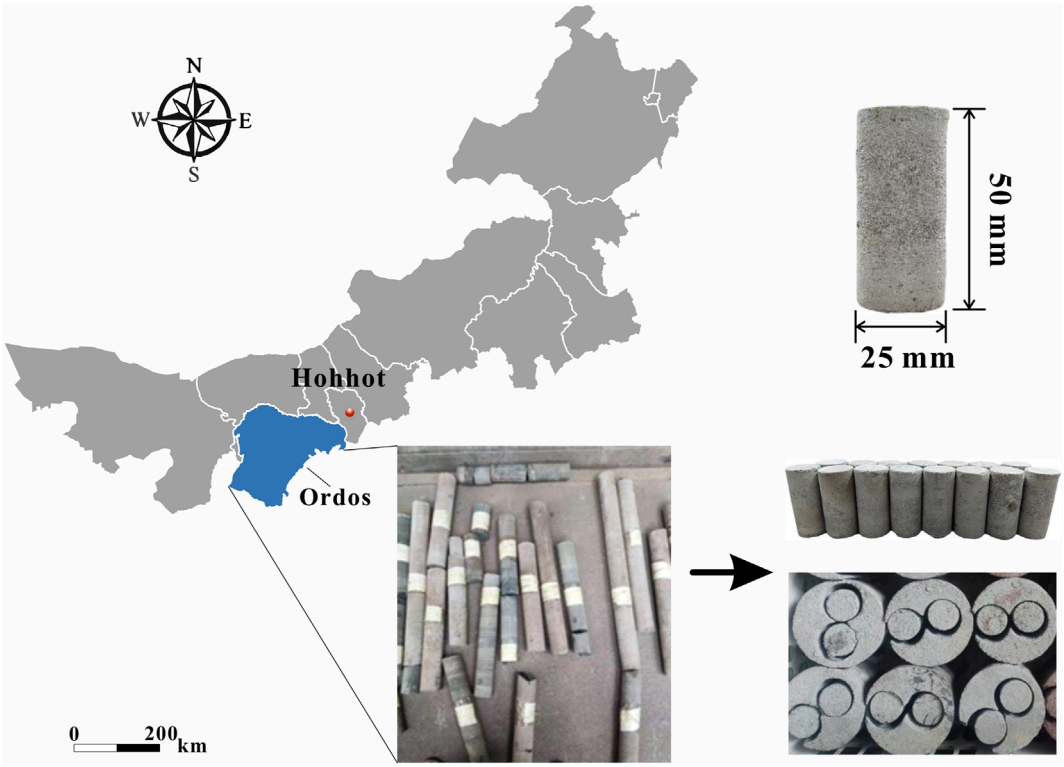

FIGURE 1
Ordos sandstone in this study.

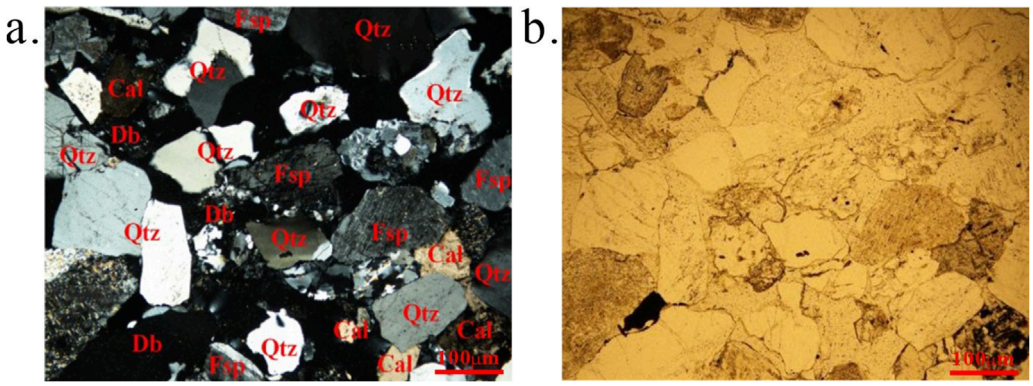

FIGURE 2
Mineral composition and microstructure of sandstone **(A)**, orthogonal polarized light; **(B)**, single polarized light Qtz: Quartz, Fsp: Feldspar, Cal: Calcite, Db: Debris).

TABLE 1 Sandstone mineral composition.

Type	Place of samples	Structure	Mineral composition			
			Quartz	Feldspar	Calcite	Debris
Sandstone	Inner Mongolia, China	Blocky	50%	30%	13.5%	6.5%

TABLE 2 Initial sample parameters: density and porosity.

Number	1	2	3	4	5	6	7	8	9	10	11
Density (g/cm^3)	1.75	1.78	1.76	1.72	1.67	1.82	1.83	1.78	1.77	1.81	1.77
Porosity	11.44	10.68	11.28	12.92	10.64	9.88	9.75	10.99	10.86	10.23	11.23
Number	12	13	14	15	16	17	18	19	20	21	
Density (g/cm^3)	1.80	1.83	1.83	1.79	1.79	1.77	1.74	1.80	1.73	1.81	
Porosity	10.51	10.59	10.28	11.28	10.96	11.47	11.53	10.13	11.39	10.66	

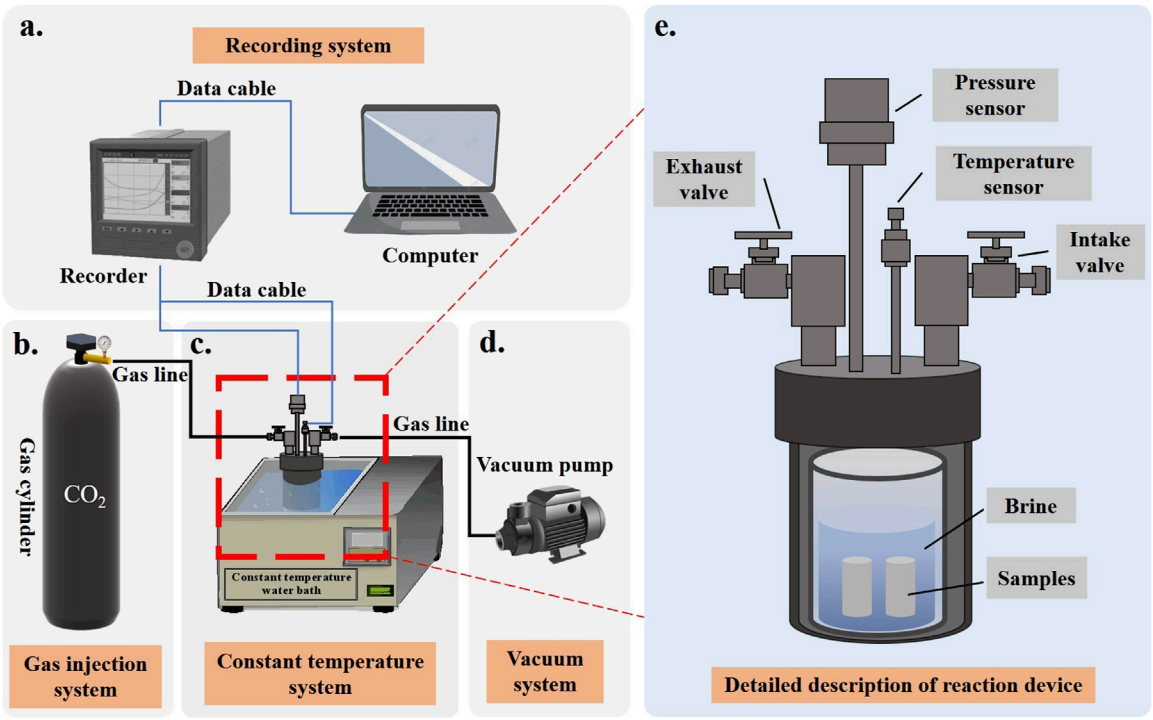

FIGURE 3
Experimental equipment and detailed diagrams (**A**, recording system; **B**, gas injection system; **C**, constant temperature system; **D**, vacuum system; **E**, detailed description of reaction device).

one cycle, and a total of five cycles were performed with reaction durations of 0 h, 12 h, 24 h, 72 h, 120 h, and 168 h, over a span of 16.5 days.

3 Results

3.1 Quality change before and after treatment

The dynamic variations in the dry mass of rock samples before and after the cyclic treatment process are key indicators for evaluating the impact of the injection cycles. Figure 5 illustrates the changes in the dry mass of the samples over time. The horizontal axis represents time, while the vertical axis displays the ratio of the mass before and after the reaction, where M_0 represents the mass of the original untreated rock sample, and M denotes the mass after the treatment. Figure 5 reveals that changes in sample mass can be divided into two distinct phases: Phase I and Phase II. During Phase I, rock samples treated with different types of saltwater show varying trends in dry mass after CO_2 injection. Specifically, samples treated with Na_2SO_4-type saline water exhibit a notable increase in mass, particularly during the second cycle, with a 0.18% increase compared to the initial state. In contrast, samples treated with NaCl-type saltwater show slight fluctuations but remain relatively stable, while samples treated with deionized water experience mass loss after CO_2 injection, decreasing by 0.12% compared to the initial state. In Phase II, with increasing cycles, all three types of saltwater-treated rock samples generally display a decrease in mass following CO_2 injection.

10.3389/fenrg.2024.1485241

TABLE 3 Test reaction parameters.

Condition	Parameter
Injection pressure	5 Mpa
Isostatic temperature	40 °C
Brine type	Na_2SO_4、NaCl、Pure water
Brine concentration	30,000 ppm
Sample number	9、8; 2、21; 17、18

Notably, NaCl-type and deionized water-treated samples show more pronounced reductions, with decreases of 0.78% and 0.67%, respectively, compared to their initial states. Although Na_2SO_4-type samples also experience mass loss, the reduction is the smallest, at only 0.21%.

3.2 Pore structure

To systematically assess the impact of cyclic CO_2 injection on pore space evolution in sandstone samples, the P/P_0 index was introduced as a metric. Here, P denotes the pore space size of the rock samples in the current treatment state, while P_0 represents the pore space of the original untreated samples. Based on pore size variations, pores were classified into three categories: macropores, mesopores, and micropores, as indicated on the horizontal axis in Figure 6.

In Figure 6, the color shading visually represents the number of cycles the samples have undergone, with darker colors indicating a higher number of cycles, up to the final count of five cycles. The pore space of the sandstone samples showed significant changes with the increase in the number of cycles. The volume of small pores generally decreased, while the volume of mesopores increased significantly and became the predominant feature of pore space changes. Although the volume of macropores also increased during cycling, it did not return to the initial level. When comparing the effects of three different brines on pore structure, the Na_2SO_4-type brine demonstrated the most notable performance. Specifically, the volume of mesopores increased most significantly during the second cycle, reaching three times the initial volume. In contrast, the NaCl-type brine had a lesser effect on mesopores, with a maximum increase of 2.5 times the initial volume, but by the fifth cycle, the mesopore volume was twice the initial volume, exceeding that of the Na_2SO_4-type brine by a factor of 1.4. The pure water type had a less pronounced effect on pore structure under cyclic CO_2 injection. The micropore volume decreased substantially, and the mesopore volume fluctuated, with a maximum increase of only 1.7 times the initial volume, lower than that observed with the other two brine types. The volume of macropores remained relatively stable throughout the cycling process, with the P/P_0 ratio fluctuating around 1, indicating minimal change. Overall, significant differences were observed in the effects of various brines on the pore structure of sandstone samples during cyclic CO_2 injection.

3.3 Longitudinal wave velocity

To examine the alterations in the homogeneity and continuity of rock samples during cyclic CO_2 injection, the wave velocity index was introduced. The evolution trend of the longitudinal wave velocity of the samples with an increasing number of cycles was visualized, as illustrated in Figure 7.

Figure 7 illustrates the relationship between time (horizontal coordinate) and longitudinal wave speed (vertical coordinate). To accurately compare differences among various brine types, the coordinate ranges were standardized across all samples. In Figure 7, the brine types, such as pure water, NaCl, and Na_2SO_4, are arranged from top to bottom. The results indicate that the variation in longitudinal wave velocity is directly influenced by the cyclic injection process, with distinct wave velocity evolution trends observed for different brine types. Specifically, for sandstone samples with pure water, the longitudinal wave velocity initially increased to 1.12 times the initial value at the start of the cycle and subsequently decreased to 0.85 times the initial value, showing a relatively straightforward trend. In contrast, for NaCl brine, a significant increase in wave velocity was observed initially, reaching 1.11 times the initial value, followed by a decrease to 0.92 times the initial value before recovering. For Na_2SO_4 brine, there was a notable increase in longitudinal wave velocity during the first three cycles, reaching 1.10 times the initial value, followed by a decrease to 0.89 times the initial value, and a subsequent rise to 1.02 times the initial value in the final phase. This pattern reflects the impact of cyclic injection on wave velocity.

3.4 Solution properties

In Figure 8, curves a, b, and c represent the changes in the concentrations of Ca^{2+}, Mg^{2+}, and K+ ions in solution over the cycling treatment time, respectively, while curve d depicts the TDS values of the solution properties. These curves illustrate the variability in solution properties during the cycling process. Initially, the concentrations of all metal ions were below 10 ppm. As the number of cycles increased, the concentration of Ca^{2+} ions rose significantly to 210.9 ppm, which is 47.1 times the initial concentration, indicating a substantial effect of cycling treatment on Ca^{2+} ions. In contrast, the concentration of Mg^{2+} ions showed an initial rapid increase followed by a decrease, eventually stabilizing at a relatively low level. The concentration of K+ ions exhibited less variation compared to Ca^{2+}, though it still showed some fluctuations relative to Mg^{2+}, highlighting its distinct trend.

The ion concentration changes in various solution systems were further analyzed. In the pure water system, the concentration of Ca^{2+} ions showed a tendency to stabilize with an increasing number of cycles. Although minor fluctuations occurred, the overall change remained limited. Conversely, the concentration of Mg^{2+} ions peaked quickly during the initial cycles and then gradually decreased, while the K+ ion concentration exhibited a slight increase initially, followed by stabilization and a small overall rise. For NaCl-type brine, the Ca^{2+} concentration peaked after four cycles, then began to decrease and eventually stabilized around 100 ppm. The Mg^{2+} ion concentration generally increased before decreasing. K^+ ions, after an initial increase, maintained stability for a period

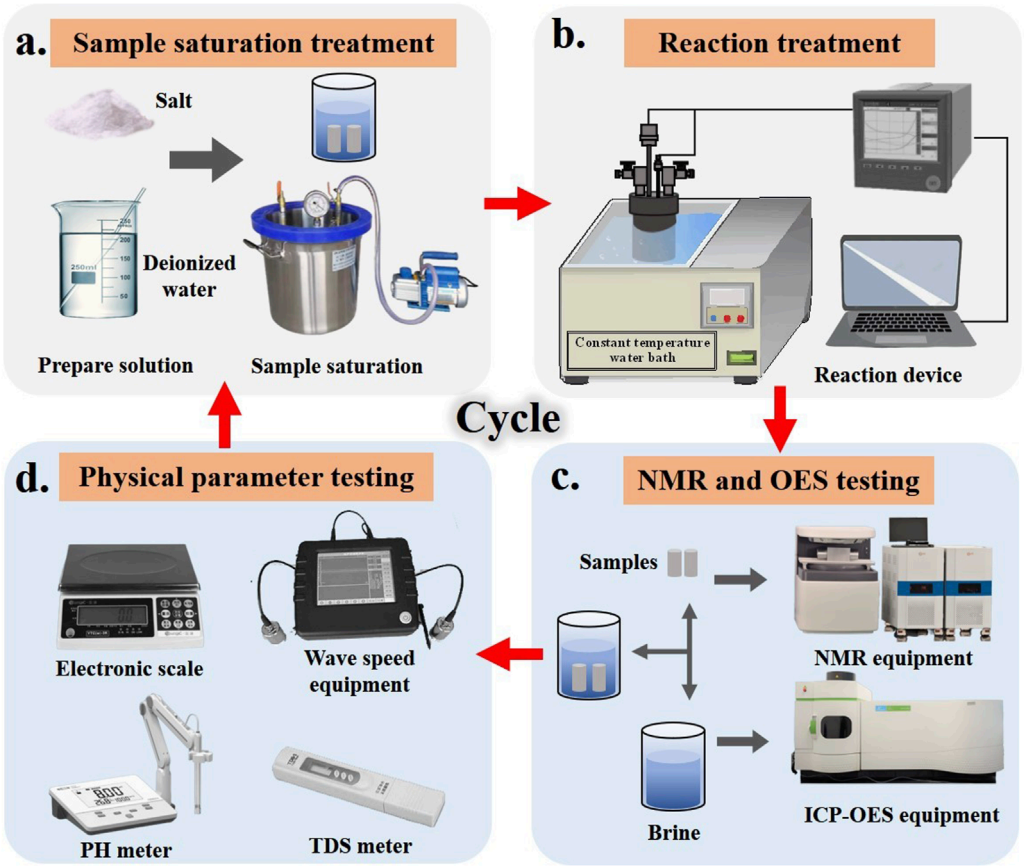

FIGURE 4
Experimental operation flow chart (**A**, sample saturation treatment; **B**, reaction treatment; **C**, NMR and OES testing; **D**, physical parameter testing).

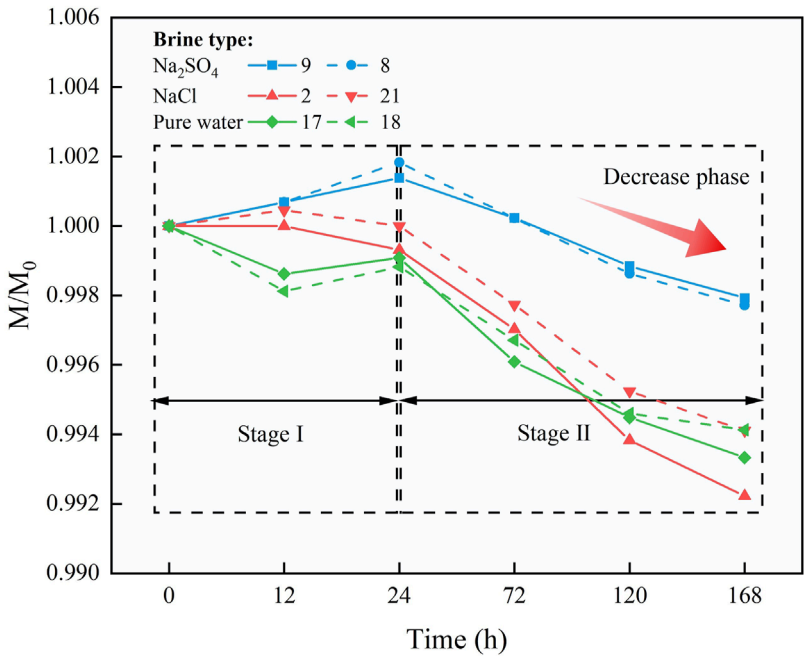

FIGURE 5
Evolution of M/M_0 with cycle time.

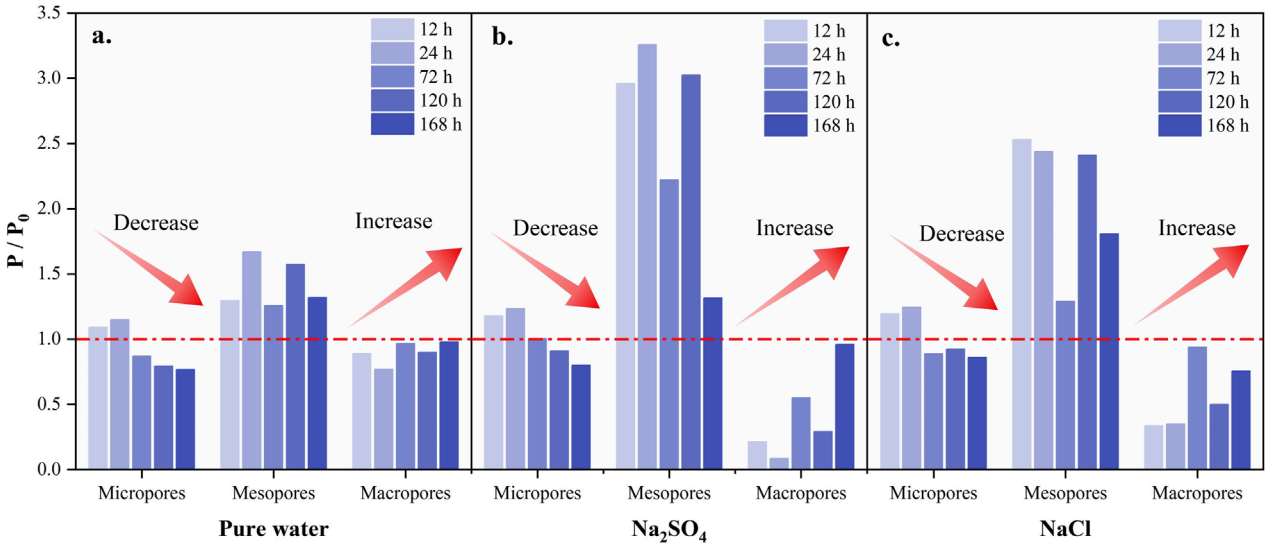

FIGURE 6
Evolution of P/P_0 with cycle time (a, b and c represent different types of salt water, **(A)** Pure water; **(B)** Na_2SO_4; **(C)** NaCl).

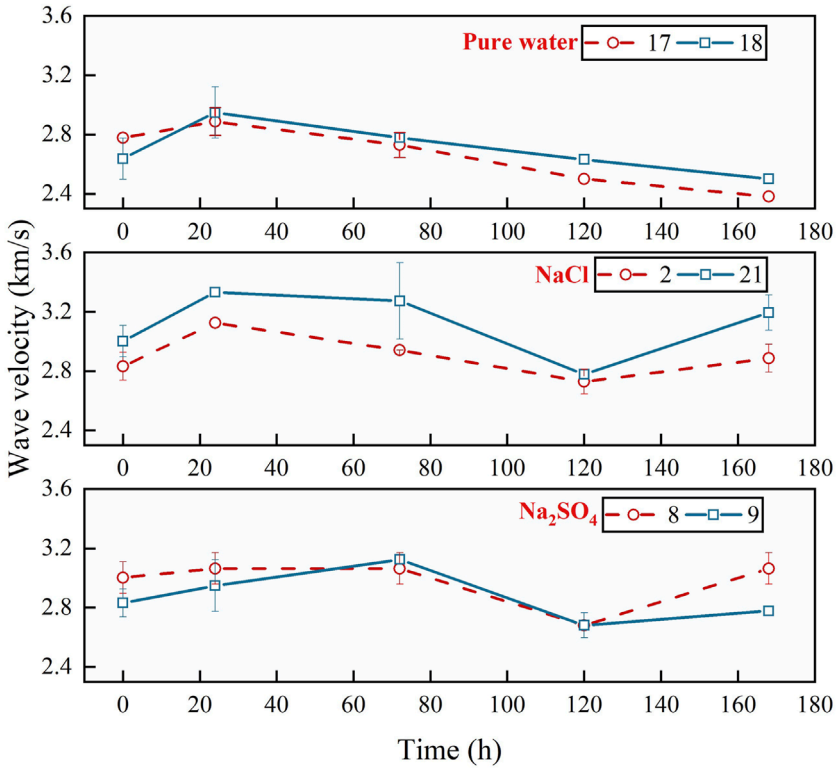

FIGURE 7
Evolution of the longitudinal wave velocity of the sample with the cycle time.

and later exhibited a more noticeable increase in concentration. In Na_2SO_4-type brines, the concentration of Ca^{2+} ions displayed more complex behavior, initially rising, then stabilizing, and finally increasing sharply. The concentration of Mg^{2+} ions increased initially, decreased, and then stabilized at double the initial concentration. The K^+ ion concentration varied more significantly, first increasing, then decreasing, and finally experiencing a rapid increase, reflecting a distinct fluctuation pattern.

In terms of total dissolved solids (TDS), the TDS values of the NaCl- and Na_2SO_4-type solutions were notably higher

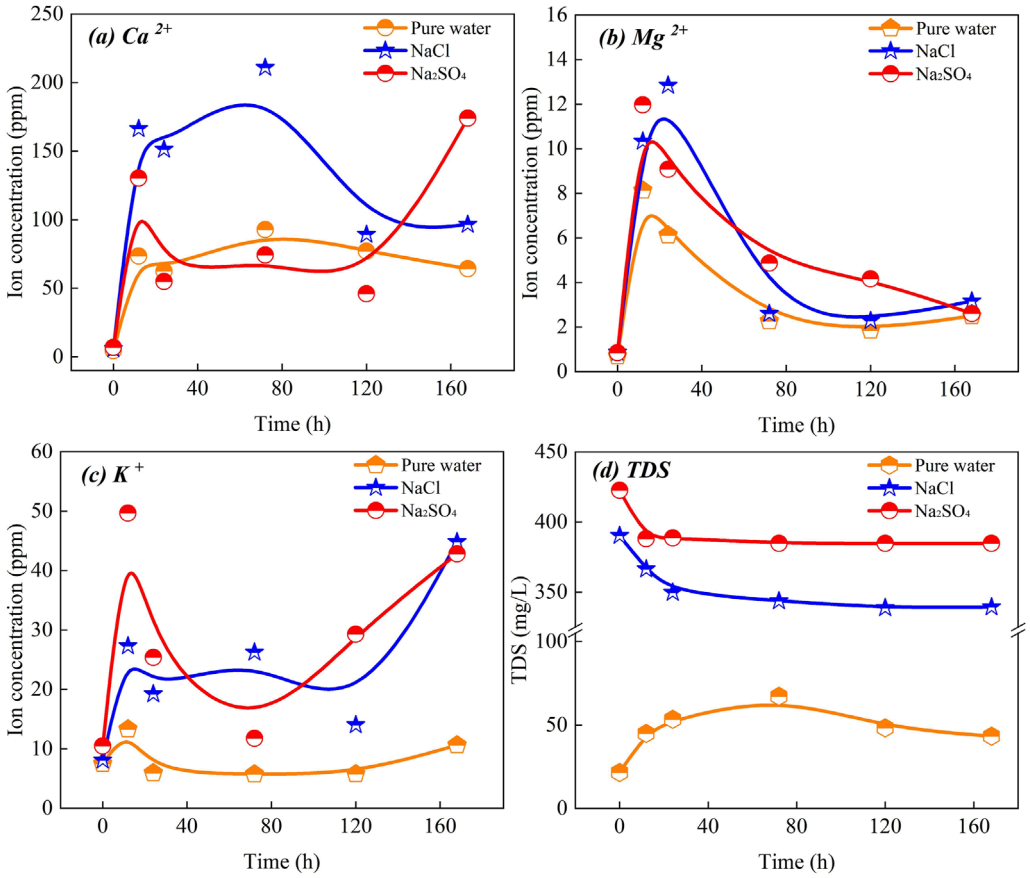

FIGURE 8
Solution characteristics change group chart **(A)**. Ca^{2+}, **(B)**. Mg^{2+}, **(C)**. K^{+}, **(D)**. TDS.

compared to the pure water-type solutions. Both NaCl and Na_2SO_4 solutions exhibited similar trends during the recirculation process, characterized by an initial rapid decline followed by a gradual decrease. In contrast, the TDS values for pure water-type solutions increased with the number of cycles and eventually stabilized, with the final values remaining higher than the initial values.

4 Discussion

4.1 Effects of CO_2 cyclic injection on solution properties

In the geological storage of CO_2, the saline aquifer serves as the crucial medium, with its primary components (sulfate, chloride, and carbonate) significantly affecting the storage efficiency (Chen et al., 2023; Wen et al., 2024). Following CO_2 injection, it rapidly dissolves in the brine, leading to quick saturation at the interface and decreasing concentration further away. This dissolution process generates carbonic acid, which substantially lowers the groundwater pH, a phenomenon known as 'acidification' (Equations 1–3). The acidification accelerates the dissolution of carbonate and some silicate minerals, releases cations such as Ca^{2+}, Mg^{2+}, and Si^{+}, and increases the concentration of HCO3- ions, thereby further enhancing the acidification process (Md Yusof et al., 2022). Additionally, the dissolved minerals and CO_2 facilitate the formation of new mineral phases (e.g., carbonate and silicate minerals), which help in CO_2 fixation but also alter the pore space. Initially, the dissolution of carbonate minerals raises the concentration of Ca^{2+} and Mg^{2+} ions, which is later reduced by reprecipitation, while the concentration of K^{+} ions remains relatively stable. Prolonged CO_2 injection lowers the solution pH, increasing the environmental acidity.

$$CO_2 + H_2O \rightarrow H_2CO_3 \quad (1)$$

$$H_2CO_3 \rightarrow H^+ + HCO_3^- \quad (2)$$

$$HCO_3^- \rightarrow H^+ + CO_3^{2-} \quad (3)$$

In sandstone minerals, the dissolution of feldspars is predominant. Feldspars undergo hydrolysis in the presence of water, releasing alkaline metal ions such as Na^{+} and K+. This process typically occurs in acidic conditions, which promote the dissolution and leaching of these metal ions from feldspars (Equations 4–6) (Luquot et al., 2016; Jayasekara et al., 2020). Clay minerals may also dissolve to some extent, forming silicate and aluminum complexes (Kweon and Deo, 2017). Although H_2SiO_4

is usually unstable, it tends to form colloidal or polymeric silicic acid in aqueous environments. This process increases the cation concentration in the solution and also leads to changes in the pore space due to the dissolution and precipitation of minerals.

$$2KAlSi_3O_8 + 9H_2O + 2H^+ \rightarrow 2K^+ + 2Al_2Si_2O_5(OH)_4 + 4H_2SiO_4 \quad (4)$$

$$2NaAlSi_3O_8 + H_2O + CO_2 \rightarrow 2Na^+ + 2Al_2Si_2O_5(OH)_4 + 4SiO_4 \quad (5)$$

$$CaAl_2Si_2O_8(s) + 2H^+ + H_2O(l) \rightarrow Ca^{2+}(aq) + Al_2Si_2O_5(OH)_4(s) \quad (6)$$

The solubility of CO_2 is significantly affected by various ionic species and their concentrations, which are primarily determined by the number of electron layers around different ions and their hydration radii (Hassanzadeh et al., 2009; Hu et al., 2013; Ali et al., 2022). As the concentration of ions such as Na^+ and K^+ increases in the solution, CO_2 solubility decreases (Chen et al., 2023). Ionized CO_3^{2-} and HCO3– are more likely to react with Ca^{2+} and Mg^{2+} ions (Equations 7, 8). SO_4^{2-} reacts with Ca^{2+} ions to form a $CaSO_4$ precipitate, a typical precipitation reaction in sulfate-type brines (Equation 9) (Wang et al., 2016). Due to the low solubility of $CaSO_4$, this reaction typically results in the formation of solid $CaSO_4$. On the other hand, the solubility of $CaCO_3$ is influenced by carbonate ion concentrations, leading to a supersaturated solution without immediate precipitation.

$$Ca^{2+}(aq) + HCO_3^-(aq) \rightarrow CaCO_3(s) + H^+ \quad (7)$$

$$Mg^{2+}(aq) + CO_3^{2-}(aq) \rightarrow MgCO_3(s) \quad (8)$$

$$Ca^{2+}(aq) + SO_4^{2-}(aq) \rightarrow CaSO_4(s) \quad (9)$$

Throughout the reaction, pore complexity increases and eventually stabilizes as minerals precipitate and dissolve. This alteration in pore structure enhances CO_2 flow ability, increases the contact area for chemical reactions, and further drives dissolution and precipitation processes. During the test, pore space complexity did not increase uniformly but fluctuated, confirming the dynamic competitive relationship between dissolution and precipitation in CO_2 geological sequestration.

4.2 Effects of CO_2 cyclic injection on sandstone pore structure

To characterize the distribution pattern of pore radius in samples subjected to cyclic injection, Figure 9 illustrates the pore radius on the horizontal axis and the pore volume ratio on the vertical axis. A vertical comparison of the plot indicates that the pore volume ratio of the bottom layer represents the initial state of the sample, with additional layers reflecting an increase in the number of cycles, up to five cycles. Based on established criteria (IUPAC), pore sizes have been categorized into three groups: macropores, mesopores (medium pores), and micropores (Thommes et al., 2015; Medina et al., 2023). Figure 9 demonstrates a clear trend in the change of pore volume share, with the primary peak (representing the most common pore size in the sample) shifting along the pore radius axis as the number of cycles increases, indicating the remodeling of the pore structure during the injection process. The shift of the primary peak toward smaller pore sizes generally signifies significant adjustment in the pore system after multiple cycles. Besides the shift in the primary peak, Figure 9 also reveals increased peak differentiation, where the boundaries between micro-, meso-, and macropores become more distinct, and the area differences between peaks progressively widen. Among the brine types tested, the Na_2SO_4 type had the most pronounced impact on pore volume ratio changes, as evidenced by the maximum shift in the primary peak. The NaCl type also significantly affected the pore structure, though to a lesser extent, while the changes observed with pure water were minimal. Following CO_2 injection, mesopore apertures became the predominant region in the pore distribution of the samples.

After ionization of Na_2SO_4 in water, SO_4^{2-} ions chemically react with mineral components of sandstone (particularly calcite, $CaCO_3$) to form insoluble sulfate precipitates (e.g., $CaSO_4$). These precipitates occlude some pores, resulting in reduced pore volume and altered pore size distribution. This high chemical reactivity is a primary factor contributing to the significant impact of Na_2SO_4-type brines on pore space. In contrast, NaCl ionizes in water to produce Na^+ and Cl^-ions, which are relatively chemically inert and engage in fewer direct reactions with sandstone minerals. Nonetheless, NaCl solutions can indirectly influence pore structure through physicochemical mechanisms such as osmotic pressure and dissolution-precipitation equilibrium. This effect, while present, is less pronounced compared to Na_2SO_4-type brines. Pure water primarily serves as a carrier for dissolved CO_2 during injection; however, CO_2 solubility is higher in pure water than in brine (Islam et al., 2016; Chen et al., 2023), which activates H+ ions in pure water control, leading to increased acidity. Additionally, the acidic environment promotes the dissolution of soluble minerals, causing changes in pore structure, as depicted in Figure 9C, where the main peak of the pore volume shifts to the left.

Figure 10 illustrates a schematic of the intricate mechanism involving salt precipitation and the shedding and dissolution of mineral crystals in the pore space, driven by differences in chemical properties under cyclic injection conditions. This process has a profound impact on pore structure evolution, making it both complex and dynamic. In the fluid transport system of saline aquifers, macropores serve as the primary pathways for fluid infiltration due to their excellent connectivity. During the transport process, detached mineral and precipitated salt crystals tend to accumulate in macropores, effectively reducing their volume and shifting the proportion of microporous space toward the mesopore range in the samples (Han et al., 2020). Furthermore, mineral crystals in small pores undergo dissolution and detachment, which not only enlarges the small pores but also facilitates their transition to the mesopore range, thus increasing pore distribution diversity (Wang et al., 2021). This explains the significant development of mesoporous regions as the number of cycles increases, resulting in a shift in the dominant pore structure feature. Significant changes in pore structure were observed within just 12 h of initial injection, with mesopores expanding more rapidly than other pore sizes, highlighting the efficiency and rapidity of the process. Overall, the interplay

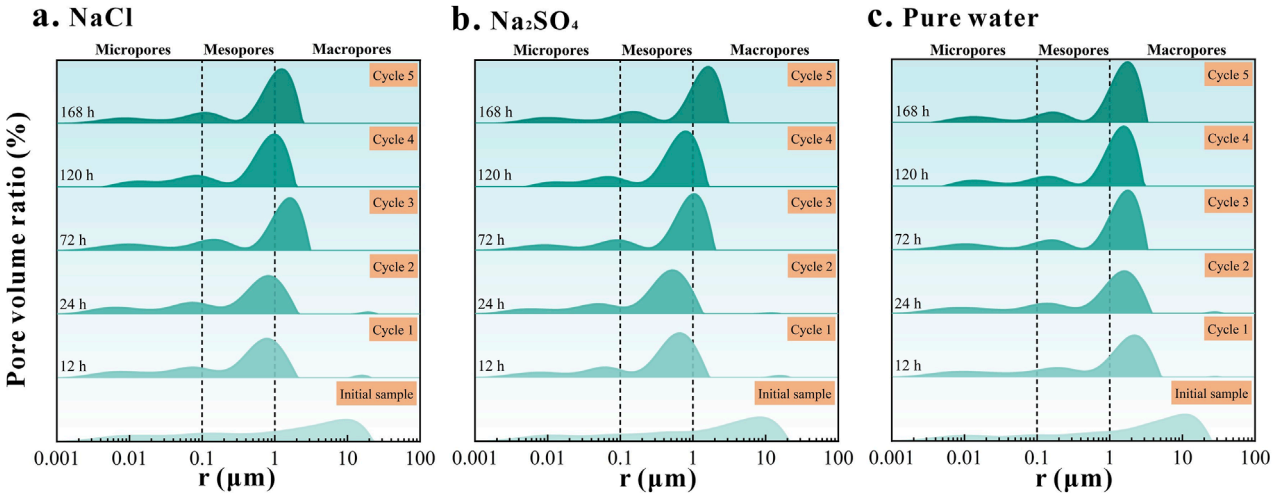

FIGURE 9
Evolution of pore radius of sandstone samples under cyclic injection conditions **(A–C)** represent different types of salt water, **(A)**. NaCl; **(B)**. Na_2SO_4; **(C)**. Pure water.

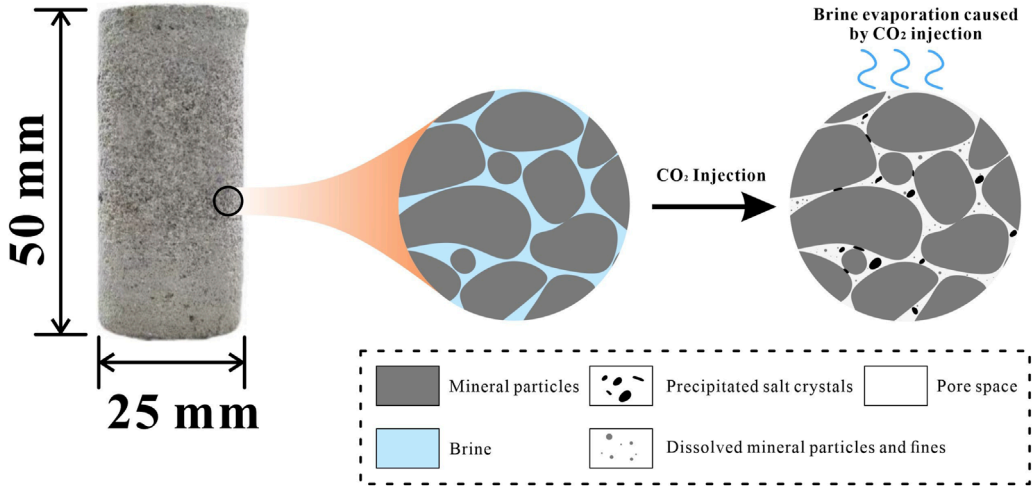

FIGURE 10
Schematic diagram of mineral crystals falling off and dissolving during injection, and pores blocked by precipitated salt crystals.

between dissolution and precipitation affects both the morphology and distribution of pore space, leading to notable fluctuations in the reservoir rock's pore structure during CO_2 injection. This understanding is essential for evaluating geological storage mechanisms, assessing storage capacity, and predicting long-term storage stability.

5 Conclusion

This paper presents a systematic investigation into the effects of CO_2 cyclic injection and sequestration processes on the microcosmic pore structure of reservoir sandstone in deep underground brackish water layers. The study employs a cyclic injection experimental approach and utilizes various techniques, including nuclear magnetic resonance (NMR), inductively coupled plasma-mass spectrometry (ICP-OES), wave velocity measurement, and solution property analysis. Sandstone samples serve as the primary research subjects to examine in detail the impact of cyclic injection on the sandstone pore structure and the chemical properties of the solution. The key research findings and conclusions are summarized as follows.

1. Following the initial CO_2 injection, the wave velocity of the sandstone samples showed a temporary increase. However, with successive cyclic injections, the wave velocity of the samples progressively decreased, indicating that the cyclic

injection process has a non-homogenizing effect on the sandstone structure.

2. During the cyclic injection process, the primary minerals in the brine solution were dissolved, leading to an expansion of small pore sizes. Concurrently, the precipitation of secondary minerals filled the larger pore spaces, causing a reduction in large pore sizes. This process alters the pore size distribution, ultimately making mesopores the predominant pore type in the sandstone samples.
3. Among the three solutions (Na_2SO_4 solution, NaCl solution, and pure water), the Na_2SO_4 solution has the most pronounced effect on the pore structure of sandstone, followed by the NaCl solution. The impact of pure water on the pore structure is comparatively minimal.
4. Under cyclic monitoring during the dynamic sequestration test, both the pore structure complexity and metal ion concentration in the sandstone samples showed a fluctuating increasing trend.

Future studies should focus on the detailed mechanisms of mineral dissolution and precipitation within sandstone reservoirs during CO_2 sequestration and their specific impacts on CO_2 sequestration effectiveness. Additionally, understanding how these mechanisms influence the long-term stability and safety of CO_2 sequestration is essential. Furthermore, integrating numerical simulation with field monitoring data will offer a more scientific and comprehensive basis for decision-making in actual projects.

Data availability statement

The original contributions presented in the study are included in the article/supplementary material, further inquiries can be directed to the corresponding author.

Author contributions

HH: Conceptualization, Data curation, Investigation, Methodology, Software, Writing–original draft, Writing–review and editing. QS: Writing–review and editing. DY: Data curation, Investigation, Methodology, Software, Supervision, Writing–review and editing. JG: Writing–review and editing. LZ: Software, Writing–review and editing. YP: Investigation, Software, Writing–review and editing.

Funding

The author(s) declare that financial support was received for the research, authorship, and/or publication of this article. This research was supported by the Major Project of Inner Mongolia Science and Technology, China (Grant No. 2021ZD0034).

Conflict of interest

The authors declare that the research was conducted in the absence of any commercial or financial relationships that could be construed as a potential conflict of interest.

Publisher's note

References

Ali, M., Yekeen, N., Ali, M., Hosseini, M., Pal, N., Keshavarz, A., et al. (2022). Effects of various solvents on adsorption of organics for porous and nonporous quartz/CO 2/brine systems: implications for CO 2 geo-storage. *Energy fuels.* 36, 11089–11099. doi:10.1021/acs.energyfuels.2c01696

Al-Khdheeawi, E. A., Vialle, S., Barifcani, A., Sarmadivaleh, M., and Iglauer, S. (2019). Effect of the number of water alternating CO2 injection cycles on CO2 trapping capacity. *APPEA J.* 59, 357. doi:10.1071/AJ18191

Aminu, M. D., Nabavi, S. A., Rochelle, C. A., and Manovic, V. (2017). A review of developments in carbon dioxide storage. *Appl. Energy* 208, 1389–1419. doi:10.1016/j.apenergy.2017.09.015

Bachu, S., and Bennion, B. (2008). Effects of *in-situ* conditions on relative permeability characteristics of CO2-brine systems. *Environ. Geol.* 54, 1707–1722. doi:10.1007/s00254-007-0946-9

Baker, H. S., Millar, R. J., Karoly, D. J., Beyerle, U., Guillod, B. P., Mitchell, D., et al. (2018). Higher CO2 concentrations increase extreme event risk in a 1.5 °C world. *Nat. Clim. Change* 8, 604–608. doi:10.1038/s41558-018-0190-1

Boampong, L. O., Tetteh, J. T., and Erzuah, S. (2023). Understanding the effects of mineral impurities, brine ionic composition and CO 2 on rock–brine–oil electrokinetic behavior using a high-salinity surface complexation model. *Energy fuels.* 37, 10200–10217. doi:10.1021/acs.energyfuels.3c01273

Chen, H., Yu, H., Zhou, B., Wang, R., Dai, Q., Qi, X., et al. (2023). Storage mechanism and dynamic characteristics of CO 2 dissolution in saline aquifers. *Energy fuels.* 37, 3875–3885. doi:10.1021/acs.energyfuels.2c03987

Dou, L., Sun, L., Lyu, W., Wang, M., Gao, F., Gao, M., et al. (2023). Trend of global carbon dioxide capture, utilization and storage industry and challenges and countermeasures in China. *Petroleum Explor. Dev.* 50, 1246–1260. doi:10.1016/S1876-3804(23)60463-X

Fang, Q., Li, Y., Peng, G., Cheng, P., and Lv, J. (2016). Effects of feldspar and salinity on the mineral sequestration capacity of CO2 in high-salinity aquifers. *Environ. Earth Sci.* 75, 1265. doi:10.1007/s12665-016-6054-y

Han, J., Han, S., Kang, D. H., Kim, Y., Lee, J., and Lee, Y. (2020). Application of digital rock physics using X-ray CT for study on alteration of macropore properties by CO2 EOR in a carbonate oil reservoir. *J. Petroleum Sci. Eng.* 189, 107009. doi:10.1016/j.petrol.2020.107009

Hassanzadeh, H., Pooladi-Darvish, M., and Keith, D. W. (2009). Accelerating CO 2 dissolution in saline aquifers for geological storage — mechanistic and sensitivity studies. *Energy fuels.* 23, 3328–3336. doi:10.1021/ef900125m

Hu, Y., Ray, J. R., and Jun, Y.-S. (2013). Na +, Ca 2+, and Mg 2+ in brines affect supercritical CO 2 –Brine–Biotite interactions: ion exchange, biotite dissolution, and illite precipitation. *Environ. Sci. Technol.* 47, 191–197. doi:10.1021/es301273g

Islam, A., Sun, A., and Lu, J. (2016). Simulating in-zone chemistry changes from injection time to longer periods of CO2 storage. *Environ. Earth Sci.* 75, 1346. doi:10.1007/s12665-016-6153-9

Jayasekara, D. W., Ranjith, P. G., Wanniarachchi, W. A. M., Rathnaweera, T. D., and Chaudhuri, A. (2020). Effect of salinity on supercritical CO2 permeability of caprock in deep saline aquifers: an experimental study. *Energy* 191, 116486. doi:10.1016/j.energy.2019.116486

Kim, S., and Santamarina, J. C. (2014). CO 2 geological storage: hydro-chemo-mechanical analyses and implications. *Greenh. Gases* 4, 528–543. doi:10.1002/ghg.1421

Kumar, R., Campbell, S., Sonnenthal, E., and Cunningham, J. (2020). Effect of brine salinity on the geological sequestration of CO 2 in a deep saline carbonate formation. *Greenh. Gases* 10, 296–312. doi:10.1002/ghg.1960

Kweon, H., and Deo, M. (2017). The impact of reactive surface area on brine-rock-carbon dioxide reactions in CO2 sequestration. *Fuel* 188, 39–49. doi:10.1016/j.fuel.2016.10.010

Luhmann, A. J., Tutolo, B. M., Bagley, B. C., Mildner, D. F. R., Seyfried, W. E., and Saar, M. O. (2017). Permeability, porosity, and mineral surface area changes in basalt cores induced by reactive transport of CO 2 -rich brine. *Water Resour. Res.* 53, 1908–1927. doi:10.1002/2016WR019216

Luquot, L., Gouze, P., Niemi, A., Bensabat, J., and Carrera, J. (2016). CO 2 -rich brine percolation experiments through Heletz reservoir rock samples (Israel): role of the flow rate and brine composition. *Int. J. Greenh. Gas Control* 48, 44–58. doi:10.1016/j.ijggc.2015.10.023

Lv, P., Song, Y., Liu, Y., Wang, B., Jiang, L., Wu, B., et al. (2017). Pore-scale imaging and analysis of phase topologies and displacement mechanisms for CO 2 -brine two-phase flow in unconsolidated sand packs. *Water Resour. Res.* 53, 9127–9144. doi:10.1002/2016WR020270

McGlade, C., and Ekins, P. (2015). The geographical distribution of fossil fuels unused when limiting global warming to 2 °C. *Nature* 517, 187–190. doi:10.1038/nature14016

Md Yusof, M. A., Mohamed, M. A., Md Akhir, N. A., Ibrahim, M. A., Saaid, I. M., Idris, A. K., et al. (2022). Influence of brine–rock parameters on rock physical changes during CO2 sequestration in saline aquifer. *Arab. J. Sci. Eng.* 47, 11345–11359. doi:10.1007/s13369-021-06110-8

Medina, B. X., Kohli, A., Kovscek, A. R., and Alvarado, V. (2023). Effects of supercritical CO 2 injection on the shale pore structures and mass transport rates. *Energy fuels.* 37, 1151–1168. doi:10.1021/acs.energyfuels.2c02254

Ou, Y., Roney, C., Alsalam, J., Calvin, K., Creason, J., Edmonds, J., et al. (2021). Deep mitigation of CO2 and non-CO2 greenhouse gases toward 1.5 °C and 2 °C futures. *Nat. Commun.* 12, 6245. doi:10.1038/s41467-021-26509-z

Seneviratne, S. I., Donat, M. G., Pitman, A. J., Knutti, R., and Wilby, R. L. (2016). Allowable CO2 emissions based on regional and impact-related climate targets. *Nature* 529, 477–483. doi:10.1038/nature16542

Seyyedi, M., Giwelli, A., White, C., Esteban, L., Verrall, M., and Clennell, B. (2020). Effects of geochemical reactions on multi-phase flow in porous media during CO2 injection. *Fuel* 269, 117421. doi:10.1016/j.fuel.2020.117421

Tang, L., Ding, G., Song, S., Wang, H., Xie, W., Zhou, Y., et al. (2023). Effect of confining pressure on CO2-brine relative permeability characteristics of sandstone in Ordos basin. *Water* 15, 4235. doi:10.3390/w15244235

Tawiah, P., Wang, H., Bryant, S. L., Dong, M., Larter, S., and Duer, J. (2021). Effects of temperature and CO2/Brine cycles on CO2 drainage endpoint phase mobility – implications for CO2 injectivity in deep saline aquifers. *Int. J. Greenh. Gas Control* 112, 103491. doi:10.1016/j.ijggc.2021.103491

Thaysen, E. M., Soler, J. M., Boone, M., Cnudde, V., and Cama, J. (2017). Effect of dissolved H2SO4 on the interaction between CO2-rich brine solutions and limestone, sandstone and marl. *Chem. Geol.* 450, 31–43. doi:10.1016/j.chemgeo.2016.11.037

Thommes, M., Kaneko, K., Neimark, A. V., Olivier, J. P., Rodriguez-Reinoso, F., Rouquerol, J., et al. (2015). Physisorption of gases, with special reference to the evaluation of surface area and pore size distribution (IUPAC Technical Report). *Pure Appl. Chem.* 87, 1051–1069. doi:10.1515/pac-2014-1117

Venkatraman, A., Dindoruk, B., Elshahawi, H., Lake, L. W., and Johns, R. T. (2017). Modeling effect of geochemical reactions on real-reservoir-fluid mixture during carbon dioxide enhanced oil recovery. *SPE J.* 22, 1519–1529. doi:10.2118/175030-PA

Wang, H., Alvarado, V., Bagdonas, D. A., McLaughlin, J. F., Kaszuba, J. P., Grana, D., et al. (2021). Effect of CO2-brine-rock reactions on pore architecture and permeability in dolostone: implications for CO2 storage and EOR. *Int. J. Greenh. Gas Control* 107, 103283. doi:10.1016/j.ijggc.2021.103283

Wang, L., He, Y., Wang, Q., Liu, M., and Jin, X. (2020). Multiphase flow characteristics and EOR mechanism of immiscible CO2 water-alternating-gas injection after continuous CO2 injection: a micro-scale visual investigation. *Fuel* 282, 118689. doi:10.1016/j.fuel.2020.118689

Wang, Z., Wang, J., Lan, C., He, I., Ko, V., Ryan, D., et al. (2016). A study on the impact of SO2 on CO2 injectivity for CO2 storage in a Canadian saline aquifer. *Appl. Energy* 184, 329–336. doi:10.1016/j.apenergy.2016.09.067

Wen, Y., Zhong, Y., Zeng, P., and Li, Q. (2024). Interfacial chemical mechanisms of brine salinity affecting the CO2 foam stability and its effect on the sequestration capacity of CO2 in deep saline aquifer. *J. Mol. Liq.* 399, 124349. doi:10.1016/j.molliq.2024.124349

Xu, L., Yue, Y., Chen, Y., Wei, P., Mo, X., and Lv, M. (2022). Effect of supercritical CO2 on limestone's pore structure based on NMR and SEM. *Pet. Sci. Technol.* 41, 1510–1525. doi:10.1080/10916466.2022.2093368

Yang, Y., Li, Y., Yao, J., Iglauer, S., Luquot, L., Zhang, K., et al. (2020). Dynamic pore-scale dissolution by CO 2 -saturated brine in carbonates: impact of homogeneous versus fractured versus vuggy pore structure. *Water Resour. Res.* 56, e2019WR026112. doi:10.1029/2019WR026112

Zhang, K., Xie, J., Li, C., Hu, L., Wu, X., and Wang, Y. (2016). A full chain CCS demonstration project in northeast Ordos Basin, China: operational experience and challenges. *Int. J. Greenh. Gas Control* 50, 218–230. doi:10.1016/j.ijggc.2016.04.025